MONTE CARLO TECHNIQUE AND HYPERCUBE SAMPLING METHOD FOR RISK ASSESSMENT AND ANALYSIS OF POWER GRID OPERATIONS

Xiaoping PENG[1,*], Ronghan ZHANG[1], Chao YAO[1], Haiyan WANG[2]

With the increasing complexity of distributed energy access and operation scenarios in the power grid, traditional Monte Carlo Simulation (MCS) faces problems of uneven sample distribution and low computational efficiency in risk assessment, making it difficult to accurately quantify the risks under the coupling of multidimensional uncertainty factors. In response to this challenge, a power grid operation risk assessment method based on improved hypercube sampling is proposed. Latin Hypercube Sampling (LHS) is used to achieve hierarchical uniform sampling, and particle swarm optimization algorithm is introduced to dynamically optimize the sample size in high-risk areas. A Monte Carlo Simulation-based Grid Operation Risk Assessment Model (MCS-GORAM) is constructed for power grid operation risk assessment. The results show that the improved method improves sample uniformity (Sobol's index 0.92) by 48.4% compared to traditional MCS, reduces convergence iteration times by 45.8%, reduces computation time by 49.4%, and reduces risk index error by only 1.23%, which is 61.7% lower than MCS. In a 500 node microgrid scenario, the expected loss of load for MCS-GORAM is 11.56 MW·h, with a prediction accuracy improvement of more than 10% compared to the comparison model. Additionally, the standard deviation of equipment failure probability estimation is reduced to 0.006, demonstrating strong robustness to high-dimensional uncertainty. Crucially, its practical applicability was further confirmed in a simulated real-world industrial microgrid case study, where it consistently maintained the highest accuracy and efficiency. The research provides an efficient quantitative tool for risk assessment of power grids containing new energy, which has important engineering application value for ensuring the safe operation of power grids and optimizing resource allocation.

Keywords: Smart grid; Risk assessment; Uncertainty handling; Artificial intelligence methods; Monte Carlo

1. Introduction

As the pace of the global energy transition accelerates, the power grid (PG) is undergoing a structural transformation from traditional centralized power generation to a deep integration of high proportion distributed energy sources such as photovoltaic power generation, wind power generation, and battery energy storage [1]. This type of complex system containing microgrids exhibits the

* Corresponding author: e-mail: 774594320@qq.com
[1] Yunnan Power Grid Co., Ltd. Electric Power Science Research Institute, Kunming, 650000, China
[2] Yunnan Power Grid Co., Ltd. Information Center, Kunming, 650000, China

characteristics of multi-energy flow coupling and dynamic evolution of operating scenarios, resulting in the interweaving of multidimensional uncertainty factors such as time-varying equipment failure probability, random meteorological disturbances, and load demand fluctuations, significantly increasing the complexity of PG operation risk assessment (RA) [2-3]. Accurately quantifying such risks is crucial for ensuring the safe operation of the PG and optimizing resource allocation. Its core lies in constructing an evaluation model that can effectively handle high-dimensional uncertainty and characterize risk propagation mechanisms [4-5].

Nafees et al. studied how to enhance security protection capabilities through situational awareness in response to advanced network attacks faced by smart grids as complex cyber physical systems, such as the Ukrainian PG attack. They summarized the current security situation from the perspective of collaborative elements, proposed a threat modeling framework, analyzed attack characteristics and technologies such as intrusion detection and mobile target defense. The results clarified the impact path of the attack on control and power systems [6]. Li et al. focused on the challenges of supply-demand balance and cost control brought about by the large-scale integration of Renewable Energy (RE) under the goal of carbon neutrality, and summarized the applications of machine learning, deep learning, and reinforcement learning in RE power system prediction, scheduling, control, and market. Research showed that Artificial Intelligence (AI) methods could effectively improve system operational efficiency [7]. Li et al. reviewed the application of Deep Reinforcement Learning (DRL) in scenarios such as smart grid scheduling and control, addressing the high uncertainty of the PG caused by the integration of RE and flexible loads. The study explored the concept, model, and technical applications of DRL, pointing out its potential in data-driven optimization operations and providing a new path for complex system control problems that traditional optimization methods are unable to address [8]. Xu et al. studied the combined risks of climate change, extreme weather, and high penetration of RE on the resilience of the PG. By analyzing data on power outages caused by hurricanes in the United States, they revealed the role of grid inertia and flexibility, and proposed strategies such as microgrids and distributed energy storage to enhance resilience. This provided empirical evidence for addressing climate risks and RE integration challenges [9].

Shahbazi et al. optimized the selection and capacity of electric vehicle charging stations (EVCS) based on Monte Carlo Simulation (MCS) modeling to address the uncertainty of losses and voltage deviations caused by their integration into the distribution network. Simulation showed that optimizing site selection could increase active/reactive power losses by 10% in most periods [10]. Erfani et al. addressed the issue of expert competence not being considered and cash flow parameter uncertainty being overlooked in wind power investment RA. They combined improved fuzzy group decision-making (considering expert competence)

with MCS to construct an integrated model of RA and cost estimation. Taking Zhongdongfeng Power Plant as an example, identifying policy and regulatory changes, raw material dependence, and market competitiveness as the main risks, it was found that uncertainty led to significant fluctuations in investment returns, emphasizing the key role of risk management in project sustainability [11]. Dwijendra et al. studied the demand side optimization coordination problem under energy market price fluctuations and achieved demand side coordination under energy market price fluctuations through two-stage optimization [12]. Xiao et al. developed an efficient probabilistic optimal power flow algorithm to address the uncertainty and correlation assessment needs of wind power integration into the grid. The generalized Johnson system was used to fit the marginal distribution, Liouville Copula was used to characterize asymmetric correlations, and grid sampling was used to generate wind power samples. The IEEE 118 node system verification showed that this algorithm significantly improved the fitting accuracy and computational efficiency compared to traditional methods, providing an advanced tool for the safety assessment of PGs with multiple wind power fields [13]. Xi et al. addressed the problem of overfitting and dimensionality reduction in traditional machine learning for detecting false data injection attacks in data collection and monitoring control systems. They combined Latin Hypercube Sampling (LHS) and reverse learning for feature selection and adopted an adaptive decision tree ensemble learning classifier. Simulation results showed that this method effectively improved generalization ability and detection accuracy [14].

In summary, many experts have conducted in-depth research on issues such as smart grid security, RE access, optimization of EVCS, and RA of wind power investment. However, there are still some shortcomings in existing research, such as insufficient application of uncertainty and correlation assessment techniques in complex systems, limited validation of emerging technologies in actual power systems, and weak evaluation of the long-term effects of improving grid resilience under extreme weather conditions. Therefore, an RA method for PG operations based on Monte Carlo techniques and LHS is proposed to achieve a dynamic balance between computational efficiency and evaluation accuracy. The innovation of the research lies in proposing a dual layer framework combining stratified sampling and intelligent optimization, constructing a multi factor coupled risk propagation model, and designing a convergence criterion based on the coefficient of variation to achieve a dynamic balance between computational efficiency and evaluation accuracy. The research aims to provide an efficient and robust risk quantification tool for complex PGs containing distributed energy.

2. Key Technical Analysis of RA for PG Operations

2.1 Ra of PG Operations Based On MCS

MCS is a numerical calculation method based on probability and statistics theory, which quantitatively evaluates the uncertainty risk of complex systems by

constructing random processes and conducting a large number of sampling experiments [15]. In the RA of power system operation, uncertain factors such as equipment failures, environmental disturbances, and load fluctuations can be included in a unified probability framework. By simulating the random changes in the operating status of the power system, the probability of risk occurrence and its impact can be accurately characterized [16]. In the scenario of PG operation, risks arise from the coupling effect of multidimensional uncertainty factors. The RA architecture of microgrids, which includes multiple power generation methods, is shown in Fig. 1.

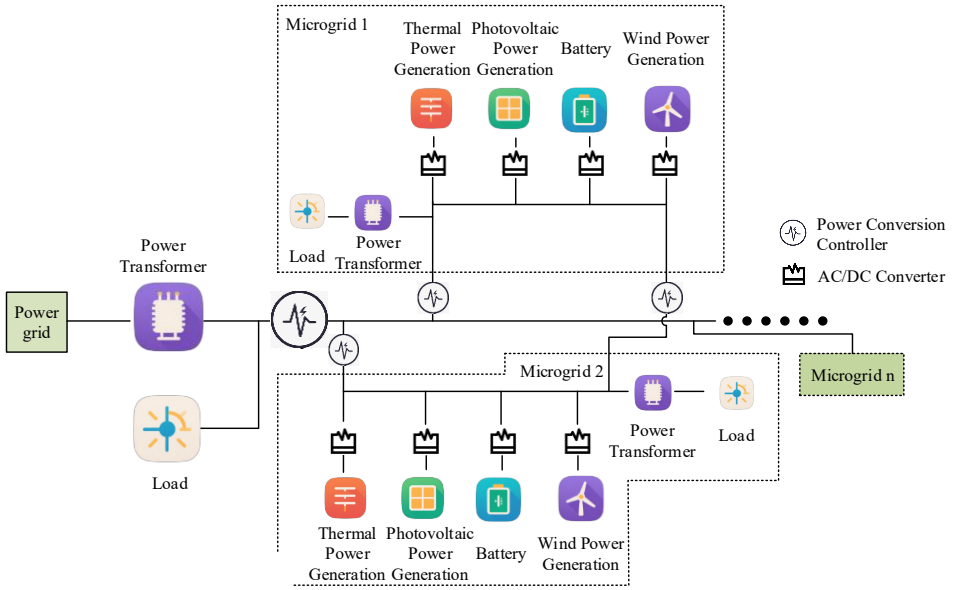

Fig. 1. RA architecture for microgrids with multiple power generation methods (Source from: Authors self drawn)

As shown in Fig. 1, the main PG is connected to various microgrids through power transformers. Each microgrid integrates various distributed energy sources such as thermal power generation, photovoltaic power generation, battery energy storage, and wind power generation. It is also equipped with loads, power transformers, AC/DC converters, and power conversion controllers, forming a complete system for energy production, storage, conversion, distribution, and consumption. In the research on RA for PG operations, MCS-based methods can model uncertain factors such as random fluctuations in distributed energy generation power, equipment failure probability, and load demand changes. The RA process for PG operations based on MCS is shown in Fig. 2.

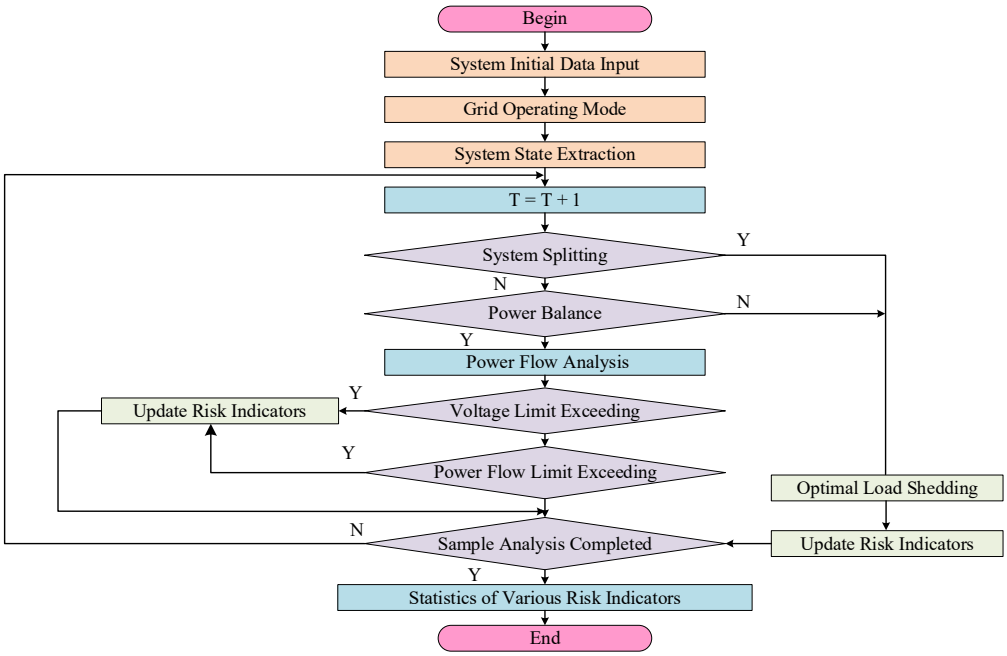

Fig. 2. RA process for PG operations based on MCS
(Source from: Authors self drawn)

As illustrated in Fig. 2, the process commences by inputting initial data into the PG system. The operator then sets the operating mode and extracts the initial state of the grid. Subsequently, the system simulates the grid's operation through iterative time steps. During each iteration, the system first checks whether a grid split has occurred. If a split is detected, it implements load reduction strategies and updates the associated risk metrics. If no split occurs, the system verifies power balance within the grid. In cases where power imbalance is identified, it reduces the load and updates the risk indicators accordingly. When power balance is achieved, the system conducts a power flow analysis to calculate node voltages and line power flows. Following this, it examines whether the calculated voltages and currents exceed their respective limits. If any limits are exceeded, the system updates the risk indicators. After each MCS cycle, the system evaluates whether the preset sample size has been reached. If the sample size is incomplete, the simulation continues. Upon completing the preset sample size, the system analyzes various risks and outputs the evaluation results [17]. The PG system contains m risk factors $X = \{X_1, X_2, \ldots, X_m\}$, each of which follows a specific probability distribution. The core of RA is to calculate risk indicator R, which is defined as the joint measurement of the probability of a risk event occurring and the severity of its consequences. The mathematical expression is shown in equation (1).

$$R = \sum_{k=1}^{n} P(E_k) \cdot \mathrm{Sev}(E_k) \tag{1}$$

In equation (1), $P(E_k)$ is the probability of occurrence of the type of risk event. $\mathrm{Sev}(E_k)$ is the severity of the consequences of this event. For a single device, its failure rate can be described using a Weibull distribution, as shown in equation (2).

$$\lambda(t) = \frac{\beta}{\eta}\left(\frac{t}{\eta}\right)^{\beta-1} \tag{2}$$

In equation (2), t is the running time of the equipment. β is the shape parameter. η is the scale parameter [18]. The aging failure probability of the equipment during the time period $[T, T+\Delta t]$ is shown in equation (3).

$$P_a = 1 - \exp\left(-\left(\left(\frac{T+\Delta t}{\eta}\right)^{\beta} - \left(\frac{T}{\eta}\right)^{\beta}\right)\right) \tag{3}$$

If meteorological factors (such as occasional failures caused by severe weather) are considered simultaneously, the comprehensive failure probability of equipment needs to be combined with a multi-factor model as shown in equation (4).

$$P_{\mathrm{f}} = 1 - (1 - P_a)(1 - P_c)(1 - P_r) \tag{4}$$

In equation (4), P_c is the probability of accidental failure caused by meteorological factors. P_r is the probability of false tripping caused by overload protection action. The risk of exceeding the limit of PG operation mainly manifests as node voltage exceeding the limit and branch power flow exceeding the limit [19]. Taking node voltage as an example, assuming that the voltage of the node i follows a normal distribution V_i, the risk value of voltage exceeding the limit is shown in equation (5).

$$R_{V_i} = P(V_i < V_{\min} \text{ ,or } V_i > V_{\max}) \cdot \mathrm{Sev}(V_i) \tag{5}$$

In equation (5), the probability of exceeding the limit $P(\cdot)$ can be calculated through the cumulative distribution function, as shown in equation (6).

$$P(V_i < V_{\min}) = \Phi\left(\frac{V_{\min} - \mu_V}{\sigma_V}\right), \quad P(V_i > V_{\max}) = 1 - \Phi\left(\frac{V_{\max} - \mu_V}{\sigma_V}\right) \tag{6}$$

In equation (6), $\Phi(\cdot)$ is the cumulative distribution function of the standard normal distribution. The severity of exceeding the limit $\mathrm{Sev}(V_i)$ is described using a conservative utility function, as shown in equation (7).

$$\mathrm{Sev}(V_i) = \begin{cases} e^{V_{\min} - V_i} - 1, & V_i < V_{\min} \\ e^{V_i - V_{\max}} - 1, & V_i > V_{\max} \end{cases} \tag{7}$$

The risk of power outage is measured by indicators such as Probability of Load Curtailment (PLC) and Expected Energy Not Provided (EENS). Assuming the system state space is Ω, the probability of each state $x \in \Omega$ occurring is $P(x)$, and the corresponding amount of load loss is $L(x)$, equation (8) can be obtained.

$$\text{PLC} = \sum_{x \in \Omega} P(x) \cdot I(L(x) > 0) \text{EENS} = \sum_{x \in \Omega} P(x) \cdot L(x) \tag{8}$$

In equation (8), $I(\cdot)$ is the indicator function. When the load loss is greater than 0, take 1; otherwise, take 0. Through the implementation process and efficiency optimization of MCS, N independent samples $\{X^{(1)}, X^{(2)}, \ldots, X^{(N)}\}$ are generated based on the probability distribution of each risk factor, the power flow equation or fault propagation model is solved for each sample $X^{(k)}$, and state variables such as node voltage, branch power flow, and load loss are obtained [20]. The sample mean, variance, and quantile of the risk indicator are calculated as shown in equation (9).

$$\begin{cases} \hat{R} = \dfrac{1}{N} \sum_{k=1}^{N} R(X^{(k)}) \\ \text{Var}(\hat{R}) = \dfrac{1}{N-1} \sum_{k=1}^{N} (R(X^{(k)}) - \hat{R})^2 \end{cases} \tag{9}$$

Finally, the convergence of the simulation is determined by the coefficient of variation $\beta = \sqrt{\text{Var}(\hat{R})} / \hat{R}$, and sampling is stopped when β is below a preset threshold. The risk propagation and classification architecture caused by key equipment failures in the distribution system is shown in Fig. 3.

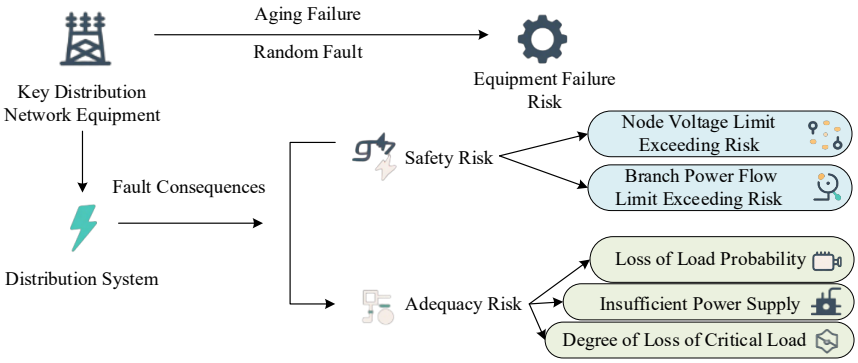

Fig. 3. Risk propagation and classification architecture caused by key equipment failures in the distribution system
(Source from: Authors self drawn)

As shown in Fig. 3, the key distribution network equipment on the left side is affected by aging faults and random faults, resulting in equipment failure risks. The consequences of these failures affect the distribution system and are decomposed into safety risks and adequacy risks. The safety risks include the risk of node voltage exceeding the limit and the risk of branch power flow exceeding the limit, reflecting the voltage stability and power flow carrying capacity of the PG operation. Adequacy risk involves the probability of load loss, insufficient power supply, and the degree of critical load loss, reflecting the ability of power supply to guarantee load demand. In the RA of PG operations based on MCS, a large number of simulated scenarios are constructed by randomly sampling uncertain factors such as equipment failure probability (such as the time distribution of aging faults, the probability of random faults), load fluctuations, and distributed energy output. Various risk indicators (such as voltage limit frequency, expected load loss, etc.) are statistically analyzed to quantify the impact of equipment failures on the safety and adequacy of the distribution system.

2.2 Construction of PG Operation RA Model Based on Improved Hypercube Sampling Method

After implementing PG operation RA based on MCS, LHS can be used instead of simple random sampling to improve computational efficiency [21]. LHS ensures uniform distribution of samples in probability space through stratified sampling, significantly reducing variance. LHS is shown in Fig. 4.

As shown in Fig. 4, the essence of hypercube sampling is to ensure uniform distribution of samples in multidimensional space through stratified sampling, avoiding the phenomenon of sample aggregation in traditional MCS. Taking LHS as an example, for one-dimensional random variable X, the LHS sample generation formula is shown in equation (10).

$$X_i = F_X^{-1}\left(\frac{i-U_i}{n}\right), \quad i=1,2,\ldots,n \tag{10}$$

In equation (10), F_X^{-1} is the inverse cumulative distribution function of X. $U_i \sim U(0,1)$ is uniformly distributed random numbers. n is the sample size [22]. For m-dimensional variable $\mathbf{X}=[X_1,X_2,\ldots,X_m]$, LHS constructs a $m\times n$ sample matrix $\mathbf{S}$, so that each row and column has only one sample, satisfying the Latin square property. If there is correlation between variables, the sample matrix needs to be orthogonalized through Cholesky decomposition, as shown in equation (11).

$$\mathbf{S}=\mathbf{L}\cdot\mathbf{L}^T \tag{11}$$

In equation (11), $\mathbf{L}$ is the lower triangular matrix. To further improve sampling efficiency, LHS is combined with Particle Swarm Optimization (PSO) algorithm to generate an initial sample matrix through LHS and calculate the risk

indicators of each sample. The study uses risk indicators as fitness functions, searches for high-risk areas through PSO and dynamically increases the sample size in that area. The sampling and optimization process is repeated until the coefficient of variation of the risk indicator $\beta \leq 5\%$ [23]. To further improve sampling efficiency, LHS is combined with PSO, and the execution process of PSO algorithm is shown in Fig. 5.

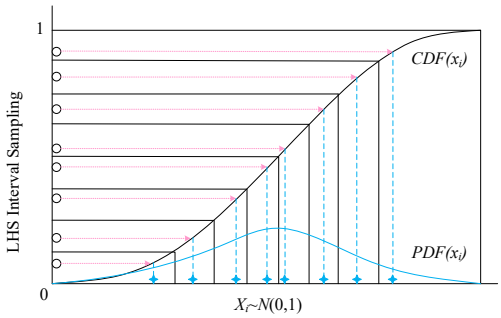

Fig. 4. LHS
(Source from: Authors self drawn)

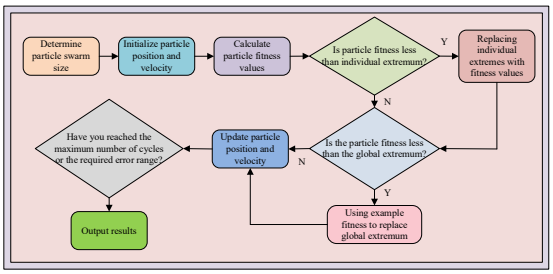

Fig. 5. Execution process of PSO algorithm
(Source from: Authors self drawn)

As depicted in Fig. 5, the algorithm begins by initializing the positions and velocities of the particles. Subsequently, it calculates the fitness values of these particles. By comparing each particle's fitness with its individual extremum and the global extremum, the algorithm dynamically updates the positions and velocities of the particles. Specifically, if a particle's fitness is superior to its individual extremum, the algorithm updates the individual extremum. If the particle's fitness also surpasses the global extremum, the algorithm updates the global extremum and guides the particles to iterate towards a more optimal solution. This iterative process persists until either the preset maximum number of cycles is reached or the error range falls within acceptable limits. Upon completion of the iterative process, the algorithm outputs the optimized sampling parameters as the final result [24-25]. In the RA of PG operations, this process utilizes the global optimization capability of PSO to iteratively optimize the key parameters of hypercube sampling, improving the sampling ability to capture uncertain factors in the PG. The particle update formula for PSO is shown in equation (12).

$$\begin{cases} v_{mt}^{k+1} = \omega v_{mt}^{k} + c_1 r_1 (x_{pbest,mt}^{k} - x_{mt}^{k}) + c_2 r_2 (x_{gbest,mt}^{k} - x_{mt}^{k}) \\ x_{mt}^{k+1} = x_{mt}^{k} + v_{mt}^{k+1} \end{cases} \tag{12}$$

In equation (12), v_{mt}^{k+1} and x_{mt}^{k} are the velocity and position of the m th particle in the k th iteration. c_1 and c_2 are learning factors. ω is the inertia weight. To visually present the differences in sample distribution characteristics between

hypercube sampling and MCS, analysis is conducted by comparing sampling data from different dimensions. The specific data is shown in Table 1.

Table 1.

MCS and hypercube sampling

Dimensions	MCS	LHS
One-dimensional	8.56, 2.13, 0.89, 4.12, 6.78, 1.34, 3.91, 5.87, 8.92, 2.95, 3.76, 1.65, 1.22, 1.45, 9.23, 4.58, 1.73, 3.21, 6.43, 0.61, 2.54, 4.82, 1.89, 7.34, 5.67, 6.21, 2.43, 2.35, 2.67, 9.11	4.89, 8.23, 4.56, 2.11, 6.98, 7.89, 0.23, 3.12, 8.34, 1.65, 7.98, 1.11, 5.32, 6.78, 2.98, 0.21, 2.01, 9.12, 7.23, 4.56, 1.34, 0.12, 8.43, 6.89, 9.01, 3.12, 4.67, 2.23, 3.21, 6.01
Two-dimensional	2.12, 5.23, 6.34, 4.11, 3.76, 4.23, 0.45, 1.67, 7.65, 3.54, 5.11, 2.65, 5.67, 4.56, 5.09, 0.11, 6.71, 3.32, 3.54, 9.43, 4.73, 3.21, 6.32, 1.11, 9.76, 4.32, 4.21, 4.43, 5.61, 8.65	0.76, 1.84, 2.03, 3.27, 4.35, 5.43, 6.05, 7.32, 8.23, 9.54, 0.83, 1.02, 2.81, 3.14, 4.02, 5.13, 6.54, 7.65, 8.76, 9.87, 0.34, 1.23, 2.45, 3.67, 4.78, 5.89, 6.91, 7.98, 8.99, 9.99

As shown in Table 1, one-dimensional data exhibits random fluctuations (such as extreme values of 0.61 and 9.23), while two-dimensional data aggregates in both low dimensional regions (such as 0.11 and 1.11) and high-dimensional regions (such as 9.76 and 9.87), reflecting the non-uniformity of simple random sampling. One-dimensional data uniformly covers the intervals of [0.12, 9.12], while two-dimensional data achieves uniform filling of the probability space through stratified sampling (with only one sample per row and column), avoiding the curse of dimensionality in MCS. The proposed model will be named MCS based Grid Operation RA Model (MCS-GORAM).

3. Experimental Design and Methods

3.1. Performance Comparison and Optimization of RA Models for PG Operations

The experiment was based on an IEEE 33 node distribution network, connected to distributed power sources and electric vehicle loads, simulating complex operating scenarios with multi-energy flow coupling. It was equipped with Intel Xeon Gold 6248 CPU (20 cores, 2.5GHz), NVIDIA Tesla V100 GPU (32GB of VRAM), and 128GB of memory, ensuring the efficiency of multi model parallel computing. The study selected the Deep Reinforcement Learning-based Grid Risk Assessment Model (DRL-GRAM), the Bayesian Network-driven Grid Operation Risk Model (BN-GORM) and the MCS-GORAM for comparison. DRL-GRAM is configured to use the deep deterministic policy gradient (DDPG) algorithm combined with a dual attention mechanism. Both the policy network and the value network are 3-layer fully connected neural networks (input layer 28 dimensions, hidden layer 128 and 64 neurons, output layer 4 dimensions and 1 dimension), learning rate 5e-4, discount factor 0.95, experience replay pool capacity 10^6, input real-time status data and historical risk indicators, output risk control actions and

level predictions; BN-GORM is configured as a Bayesian network with 50 nodes (10 basic variables, 25 intermediate variables, 15 risk events), learns dependencies through the MMHC algorithm, trains conditional probability tables by maximum likelihood estimation, and reasoning by variable elimination method. It inputs real-time monitoring and historical fault data, and outputs risk probability and critical path. The response delay comparison of different models is shown in Fig. 6.

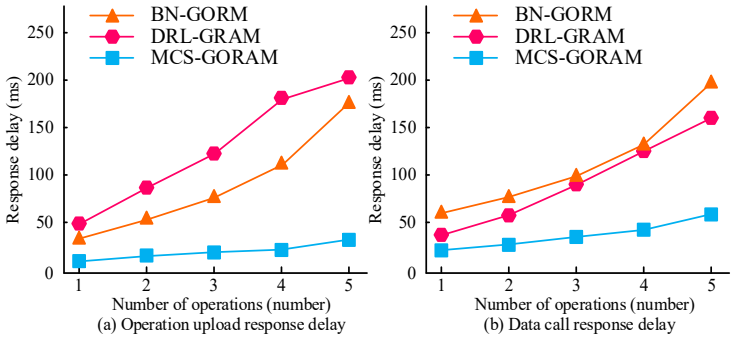

Fig. 6. Comparison of response delay among different models
(Source from: Authors self drawn)

In Fig. 6 (a), as the number of operations increased from 1 to 5, the response delay of all three models showed an upward trend. Among them, the response delay growth of the MCS-GORAM model was the smoothest, significantly lower than that of the BN-GORM and DRL-GRAM models. In Fig. 6 (b), as the number of operations increased, the response delay of the MCS-GORAM model remained lower than the other two models. This indicated that the MCS-GORAM model could maintain lower response latency when handling more operations, whether in operation upload or data call scenarios. The comparison of training errors and losses for different evaluation models is shown in Fig. 7.

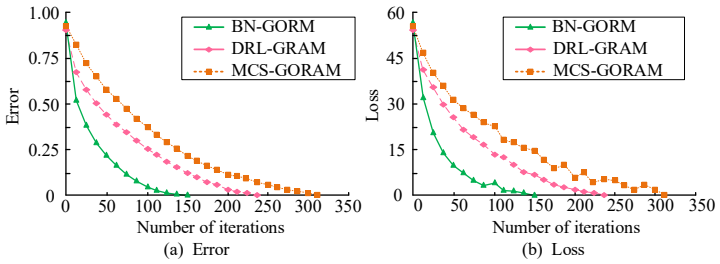

Fig. 7. Comparison of training error and loss for different evaluation models
(Source from: Authors self drawn)

In Fig. 7 (a), as the iteration count increased, the errors of all three models showed a decreasing trend. Among them, the MCS-GORAM model had the fastest error reduction rate and the lowest final error value, significantly better than the

BN-GORM and DRL-GRAM models, reflecting its advantage in error convergence. In Fig. 7 (b), the loss value of the MCS-GORAM model also decreased the most rapidly and remained lower than the other two models during the iteration process, indicating that it performed better in parameter optimization and loss function minimization. This result validated that the MCS-GORAM model could more efficiently approximate the true risk distribution during training. By combining hypercube sampling with MCS, the prediction error and training loss of the model were effectively reduced, and the accuracy and stability of RA were improved. The performance comparison of RA methods for PG operations is shown in Table 2.

Table 2

Performance comparison of RA methods for PG operations

Performance indicator	MCS	LHS	Improved hypercube sampling (LHS+IPSO)
Sample uniformity (Sobol' Index)	0.62	0.89	0.92
Convergence iterations	1200	800	650
Computation time (s)	45.23	28.76	22.45
Risk indicator error (%)	3.21	1.89	1.23
Equipment failure probability (λ)	0.052 ± 0.013	0.051 ± 0.008	0.050 ± 0.006
Node voltage violation probability (P_V)	0.085 ± 0.012	0.083 ± 0.009	0.082 ± 0.007
Branch power flow violation probability (P_S)	0.068 ± 0.011	0.065 ± 0.007	0.063 ± 0.005
Expected energy not supplied (EENS, MW·h)	12.34 ± 2.12	11.87 ± 1.56	11.56 ± 1.23
Probability of energy shortage (P_E)	0.12 ± 0.03	0.10 ± 0.02	0.09 ± 0.01

As shown in Table 2, in terms of sample uniformity, LHS and its improved methods significantly increased the coverage of samples in multidimensional probability space through stratified sampling and intelligent optimization (Sobol's index reached 0.89-0.92), avoiding sample aggregation of MCS (index only 0.62), and ensuring comprehensive capture of risk factors. In terms of convergence and efficiency, the convergence iteration times of LHS+IPSO were reduced by 45.8% (650 times vs. 1200 times for MCS), and the computation time was reduced by 49.4% (22.45 svs. 45.23 seconds), reflecting the high efficiency of the combination of hierarchical sampling and PSO algorithm, especially suitable for high-dimensional PG scenarios with distributed energy. In terms of risk accuracy, the improved method reduced the risk indicator error (1.23%) by 61.7% compared to MCS, and the standard deviation of the estimated values for key risks such as equipment failure, voltage/flow exceeding limits, and insufficient power was smaller (such as the standard deviation of λ decreasing from 0.013 to 0.006),

indicating that it quantified uncertainty factors more stably. The calculation accuracy of Expected Loss of Load (EENS) improved by 14.4% (11.56 vs. 12.34 MW • h), verifying the advantages of improved hypercube sampling in complex PG RA.

3.2 Analysis of Feature Extraction Accuracy and Computational Cost of PG RA Model

To further validate the superiority of the model, the study continued to introduce the Graph Neural Network Enhanced Grid Topology RA Model (GNN-GTRAM), and the experimental outcomes are presented in Fig. 8.

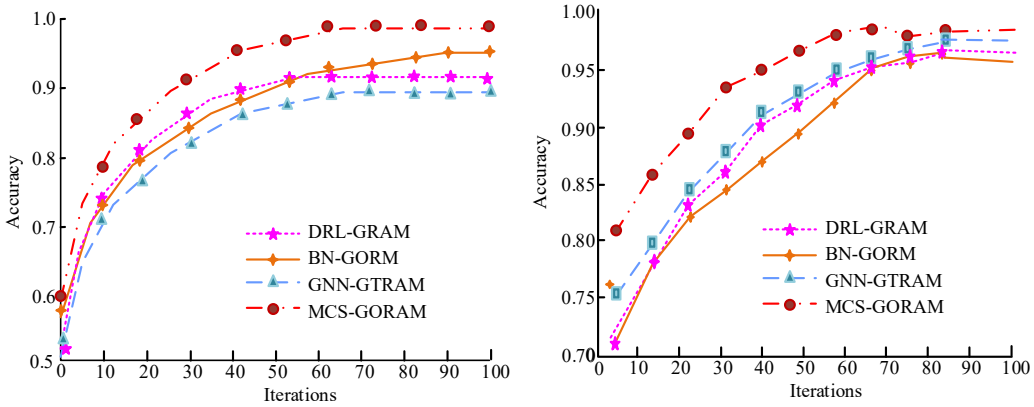

(a) Changes in accuracy of feature extraction in key areas of the power grid

(b) Changes in the accuracy of global feature extraction in the power grid

Fig. 8. Comparison of accuracy in feature extraction of PG
(Source from: Authors self drawn)

In Fig. 8 (a), as the iteration count increases, the accuracy of the MCS-GORAM model improved the most significantly, and the final accuracy was higher than that of the DRL-GRAM, BN-GORM, and GNN-GTRAM models, reflecting its advantage in feature extraction in key regions. In Fig. 8 (b), the global feature extraction accuracy of MCS-GORAM grew rapidly and consistently led, indicating its stronger ability to capture the overall characteristics of the PG. By combining MCS with hypercube sampling, MCS-GORAM exhibited higher accuracy and faster convergence speed in both local (key regions) and global feature extraction, effectively improving the accuracy of RA.

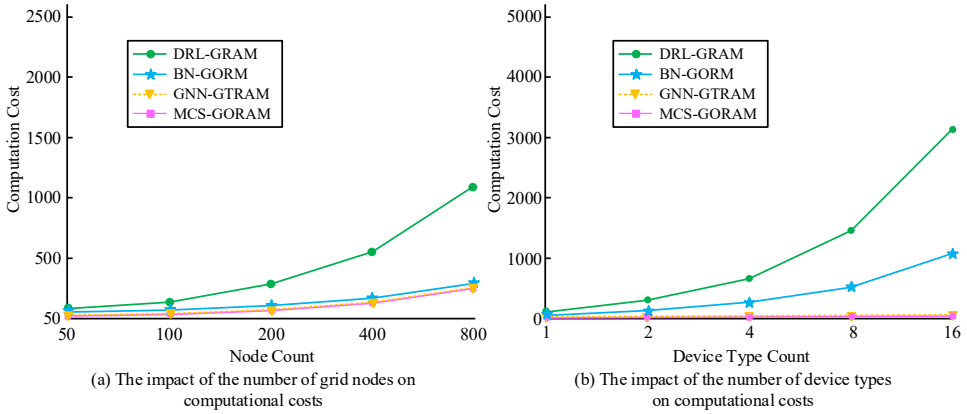

Fig. 9. Comparison of the impact of grid scale and equipment complexity on calculation costs (Source from: Authors self drawn)

In Fig. 9 (a), as the number of grid nodes increased from 50 to 800, the MCS-GORAM model showed the smallest increase in computational cost, significantly lower than the DRL-GRAM, BN-GORM, and GNN-GTRAM models. This indicated that MCS-GORAM utilized hypercube sampling to optimize sample distribution, reduce invalid simulations, and efficiently handle large-scale PG node scenarios, while maintaining low computational costs during PG expansion. In Fig. 9 (b), as the number of device types increased from 1 to 16, the computational cost of MCS-GORAM remained stable and much lower than other models. The multi-scenario performance comparison of the RA model for PG operations is shown in Table 3.

Table 3

Comparison of multi scenario performance of RA models for PG operations

Scenario	Model	Risk indicator error (%)	Convergence time (s)	Sample utilization (%)	Equipment fault prediction accuracy (%)	Voltage violation prediction accuracy (%)
Small-scale distribution network (33Nodes)	MCS-GORAM	1.23	18.45	92.3	95.6	94.8
	DRL-GRAM	2.15	25.67	85.2	90.3	89.5
	BN-GORM	1.87	22.34	88.5	92.1	91.2
	GNN-GTRAM	1.98	23.76	87.6	91.8	90.8
Medium-scale transmission network (118Nodes)	MCS-GORAM	1.56	32.78	90.1	94.2	93.5
	DRL-GRAM	2.89	40.12	78.3	87.6	86.4
	BN-GORM	2.34	36.54	83.4	90.5	89.1
	GNN-GTRAM	2.56	38.23	81.7	89.3	88.2
Large-scale microgrid Cluster (500Nodes)	MCS-GORAM	1.89	45.32	88.7	93.1	92.6
	DRL-GRAM	3.56	55.43	72.5	85.2	84.3
	BN-GORM	2.98	50.12	79.6	88.9	87.5
	GNN-GTRAM	3.12	52.34	76.8	87.8	86.7

In a small-scale distribution network (33 nodes), the MCS-GORAM model performed the best, with a risk index error of 1.23%, convergence time of 18.45 seconds, sample utilization rate of 92.3%, equipment fault prediction accuracy of 95.6%, and voltage limit prediction accuracy of 94.8%. In contrast, DRL-GRAM was slightly inferior in both accuracy and time, especially in predicting voltage exceeding limits with an accuracy of 89.5%. For medium-sized transmission networks (118 nodes), MCS-GORAM still led with a risk index error of 1.56%, convergence time of 32.78 seconds, equipment failure prediction accuracy of 94.2%, and voltage limit prediction accuracy of 93.5%. The performance of DRL-GRAM was relatively low, especially in terms of convergence time and sample utilization. In the scenario of a large-scale microgrid cluster (500 nodes), MCS-GORAM continued to perform well, with a risk index error of 1.89%, convergence time of 45.32 seconds, sample utilization rate of 88.7%, equipment fault prediction accuracy of 93.1%, and voltage limit prediction accuracy of 92.6%. DRL-GRAM performed relatively poorly in this scenario, with a voltage limit prediction accuracy of only 84.3%.

3.3 Real-World Case Study Verification

To further validate the practical applicability and robustness of the proposed MCS-GORAM model, a case study based on a simulated real-world regional microgrid was introduced. This microgrid, modeled after an industrial park in East China, features a 45-node distribution network. It integrates a high penetration of renewable energy sources, including 10 MW of photovoltaic (PV) generation and 5 MW of wind power, supported by a 2 MWh Battery Energy Storage System (BESS). The load profile is characterized by a mix of critical industrial machinery and standard commercial consumption, exhibiting higher volatility and more complex correlations than the standardized IEEE test system. The performance of all models in this case study is presented in Table 4.

Table 4

Performance Comparison in real-world microgrid - case study

Model	Risk indicator error (%)	Convergence time (s)	Sample utilization (%)	Equipment fault prediction accuracy (%)	Voltage violation prediction accuracy (%)
MCS-GORAM	1.48	24.12	90.5	94.1	93.3
DRL-GRAM	2.95	36.45	79.1	88.2	87.0
BN-GORM	2.41	31.88	84.6	90.3	89.4
GNN-GTRAM	2.65	34.02	82.3	89.5	88.6

As shown in Table 4, it indicates that MCS-GORAM continues to demonstrate superior performance even in this complex, real-world scenario. It achieved the lowest risk indicator error (1.48%) and the fastest convergence time (24.12 s), outperforming the next best model, BN-GORM, by a significant margin. While the absolute performance metrics for all models slightly decreased compared

to the idealized IEEE 33-bus system due to the increased complexity and uncertainty, the relative advantage of MCS-GORAM remained robust. This suggests that the efficiency and accuracy gains from the improved hypercube sampling method hold up well when faced with the higher volatility and non-standard characteristics of actual operational data, confirming its strong potential for practical engineering applications.

4. Conclusion

With the transformation of the PG towards a high proportion of distributed energy (photovoltaic, wind power, energy storage) and a multi-energy flow coupling mode, the RA of PG operations face multidimensional uncertainty challenges such as time-varying probability of equipment aging and failure, meteorological interference, and load fluctuations. Traditional MCS suffers from sample aggregation and curse of dimensionality caused by random sampling, making it difficult to achieve high-precision quantification of risk indicators within reasonable computational costs. To this end, a MCS-GORAM based on LHS and PSO optimization was proposed, which improved the uniformity of the sample space through stratified sampling and dynamically adjusted the sampling density for high-risk areas, achieving collaborative optimization of computational efficiency and evaluation accuracy. Experimental data showed that in the IEEE 33 node distribution network scenario, the sample uniformity index (Sobol 'index) of MCS-GORAM reached 0.92, which was 48.4% higher than the traditional MCS (0.62). The convergence iteration times were reduced from 1200 to 650, and the computation time was reduced by 49.4% (22.45 seconds). The error rate of risk indicators was only 1.23%, and the standard deviation of equipment failure probability estimation was reduced to 0.006. In the large-scale microgrid cluster (500 nodes) test, the expected loss of load of the model was 11.56 MW • h, which was 12.5% lower than DRL-GRAM. The sample utilization rate reached 88.7%, the equipment failure prediction accuracy was 93.1%, and the voltage limit prediction accuracy was 92.6%, demonstrating efficient adaptability to large-scale scenarios. Most importantly, to obtain conclusions that are practically usable, a case study based on a concrete industrial microgrid was conducted. The results confirmed that the model’s robust performance and efficiency advantages are maintained in a non-idealized operational environment, underscoring its significant value for real-world applications. The research was limited by the lack of a dynamic correlation model for equipment cascading failures under extreme weather conditions. Future research will introduce a fault propagation model based on spatiotemporal networks to quantify the probability of multiple equipment cascading failures. Combining Copula theory, a nonlinear correlation network will be constructed to enhance the

characterization ability of complex coupling risks, in order to support real-time risk management and resilience improvement of the new power system.

REFERENCES

[1] *George A. S., Baskar T., Srikaanth P. B.* Cyber threats to critical infrastructure: assessing vulnerabilities across key sectors. Partners Universal International Innovation Journal, 2024, 2(1): 51-75.

[2] *Singh M. P., Sinha N.* Data creation techniques and data-oriented models for dynamic security assessment of power system. Electrical Engineering, 2024, 106(5): 5787-5800.

[3] *Tiwari S., Kumar A.* Advances and bibliographic analysis of particle swarm optimization applications in electrical power system: concepts and variants. Evolutionary Intelligence, 2023, 16(1): 23-47.

[4] *Veers P., Bottasso C. L., Manuel L., Naughton J., Pao L., Paquette J., Rinker J.* Grand challenges in the design, manufacture, and operation of future wind turbine systems. Wind Energy Science, 2023, 8(7): 1071-1131.

[5] *Mallapragada D. S., Dvorkin Y., Modestino M. A., Esposito D. V., Smith W. A., Hodge B. M., Taylor A. D.* Decarbonization of the chemical industry through electrification: Barriers and opportunities. Joule, 2023, 7(1): 23-41.

[6] *Nafees M. N., Saxena N., Cardenas A., Grijalva S., Burnap P*. Smart grid cyber-physical situational awareness of complex operational technology attacks: A review. ACM Computing Surveys, 2023, 55(10): 1-36.

[7] *Li Y., Ding Y., He S., Hu F., Duan J., Wen G., Zeng Z.* Artificial intelligence-based methods for renewable power system operation. Nature Reviews Electrical Engineering, 2024, 1(3): 163-179.

[8] *Li Y., Yu C., Shahidehpour M., Yang T., Zeng Z., Chai T.* Deep reinforcement learning for smart grid operations: Algorithms, applications, and prospects. Proceedings of the IEEE, 2023, 111(9): 1055-1096.

[9] *Xu L., Feng K., Lin N., Perera A. T. D., Poor H. V., Xie L., OMalley M*. Resilience of renewable power systems under climate risks. Nature Reviews Electrical Engineering, 2024, 1(1): 53-66.

[10] *Shahbazi A., Moradi CheshmehBeigi H., Abdi H., Shahbazitabar M.* Probabilistic optimal allocation of electric vehicle charging stations considering the uncertain loads by using the Monte Carlo simulation method. Journal of Operation and Automation in Power Engineering, 2023, 11(4): 277-284.

[11] *Erfani A., Tavakolan M.* Risk evaluation model of wind energy investment projects using modified fuzzy group decision-making and Monte Carlo simulation. Arthaniti: Journal of Economic Theory and Practice, 2023, 22(1): 7-33.

[12] *Dwijendra N. K. A., Arsana I. G. N. K., Al-Hawary S. I. S., Prakaash A. S., Parra R. M. R., Jalil A. T., Hammid A. T.* Operation of the multiple energy system with optimal coordination of the consumers in energy market. Rigas Tehniskas Universitates Zinatniskie Raksti, 2023, 27(1): 1-13.

[13] *Xiao Q., Tan Z., Du M.* Probabilistic optimal power flow computation for power grid including correlated wind sources. IET Generation, Transmission & Distribution, 2024, 18(14): 2383-2396.

[14] *Xi L., Tian X., He M., Cheng C.* False Data Injection Detection in Power System Based on LOSSA-AdaBoostDT. Protection and Control of Modern Power Systems, 2025, 10(3): 55-64.

[15] *Onukwulu E. C., Agho M. O., Eyo-Udo N. L.* Developing a framework for predictive analytics in mitigating energy supply chain risks. International Journal of Scholarly Research and Reviews, 2023, 2(2): 135-155.

[16] *Ashok Babu P., Mazher Iqbal J. L., Siva Priyanka S., Jithender Reddy M., Sunil Kumar G., Ayyasamy R.* Power control and optimization for power loss reduction using deep learning in microgrid systems. Electric Power Components and Systems, 2024, 52(2): 219-232.
[17] *Tan J., He Z., Wang X*. Extensible grid sampling for quantile estimation. Mathematics of Computation, 2025, 94(352): 763-800.
[18] *Li X., Wang J., Yang C.* Risk prediction in financial management of listed companies based on optimized BP neural network under digital economy. Neural Computing and Applications, 2023, 35(3): 2045-2058.
[19] *Gan Y., Huang J., Wu J., Lü H., Chen J., Cai H., Du Z.* Research on probabilistic power flow calculation improvement method of power system including wind and photovoltaic power generation. Journal of Electric Power Science and Technology, 2024, 38(5): 34-43.
[20] *Wu Q. H., Bose A., Singh C., Chow J. H., Mu G., Sun Y., Liu Y.* Control and stability of large-scale power system with highly distributed renewable energy generation: viewpoints from six aspects. CSEE Journal of Power and Energy Systems, 2023, 9(1): 8-14.
[21] *Chen W., Liu Z., Wei Z., Shi J., Xun Z.* SSO risk evaluation method for grid-connected wind farm systems based on LHS and extended Prony. Electrical Engineering, 2023, 105(2): 853-865.
[22] *Khalid H. M., Qasaymeh M. M., Muyeen S. M., El Moursi M. S., Foley A. M., Sweidan T. E. O., Sanjeevikumar P.* WAMS operations in power grids: A track fusion-based mixture density estimation-driven grid resilient approach toward cyberattacks. IEEE Systems Journal, 2023, 17(3): 3950-3961.
[23] *Jalilian M., Rastgou A., Kharrati S., Hosseini-Hemati S.* Frequency stability of hybrid power system in the presence of superconducting magnetic energy storage and uncertainties. Journal of Operation and Automation in Power Engineering, 2023, 11(4): 230-239.
[24] *Chen J., Henry E., Jiang X*. Is cybersecurity risk factor disclosure informative? Evidence from disclosures following a data breach. Journal of Business Ethics, 2023, 187(1): 199-224.
[25] *Kabeyi M. J. B., Olanrewaju O. A.* Smart grid technologies and application in the sustainable energy transition: a review. International Journal of Sustainable Energy, 2023, 42(1): 685-758.